第37卷第3期
2018年6月

红外与毫米波学报
J. Infrared Millim. Waves

Vol. 37, No. 3
June, 2018

文章编号: 1001-9014(2018)03-0269-06

DOI: 10.11972/j.issn.1001-9014.2018.03.003

Semi-circularly folded microstrip meander line slow-wave structure for Ka-band traveling-wave tube with cylindrical electron beam

DING Chong*, LI Qian, LEI Xia, WU Gang-Xiong, YANG Rui-Chao, GONG Yu-Bin, WANG Wen-Xiang, WEI Yan-Yu*

(National Key Laboratory of Science and Technology on Vacuum Electronics, School of Physical Electronics, University of Electronic Science and Technology of China, Chengdu, 610054, China)

Abstract: A folded microstrip meander line (FMML) slow-wave structure (SWS) based on slotted dielectric substrate is proposed. Due to the metal meander line printed in a semi-circular slot of the dielectric substrate, the proposed FMML SWS is very suitable for traveling-wave tubes (TWT) with cylindrical electron beam (CEB), which can be focused by a traditional periodic permanent (PPM) magnetic focusing system. The analyses of dispersion characteristics, coupling impedances, transmission properties and particle-in-cell (PIC) of the proposed FMML SWS are investigated. Compared with traditional planar microstrip meander line (PMML) SWS, the FMML SWS has the advantages of lower phase velocities, weaker dispersion and higher coupling impedances, which make the FMML SWS suitable for developing low-voltage, wideband and miniature millimeter-wave TWTs. With a focus magnetic of only 0.4 T, a Ka band TWT with the FMML SWS is capable of delivering 42.32 W output power with a corresponding gain of 26.26 dB at 35 GHz, while the voltage and the current of the electron beam are set to be 6 550 V and 0.1 A, respectively.

Key words: Electron physics, folded microstrip meander line (FMML), computer simulation, slow wave structure (SWS), traveling wave tubes (TWT).

PACS: 42.72.Ai, 84.40.Fe, 84.47.+w, 84.40.Az

适用于 Ka 波段圆形电子注行波管的半圆形卷绕微带线慢波结构

丁 冲*, 李 倩, 雷 霞, 吴钢雄, 杨睿超, 宫玉彬, 王文祥, 魏彦玉*

(微波电真空器件国家重点实验室, 物理电子学院, 电子科技大学, 四川 成都 610054)

摘要: 提出了一种基于开槽介质基底的卷绕微带线慢波结构. 由于金属曲折微带线印制在介质基底的半圆形槽中, 这种卷绕微带线慢波结构非常适合圆形电子注行波管, 从而使得采用这种新型慢波结构的行波管可以利用传统的周期永磁磁场进行聚焦. 文章对提出的卷绕微带线慢波结构的色散特性, 耦合阻抗, 传输特性及注-波互作用进行了分析. 和传统的平面微带线慢波结构相比, 提出的卷绕微带线慢波结构具有更低的相速、更弱的色散和更高的耦合阻抗, 从而使得其适合于低电压、宽频带、小型化的毫米波行波管. 将同步电压及直流电流分别设置为 6550 V 及 0.1 A 的情况下, 基于该卷绕微带线慢波结构的 Ka 波段行波管在 35 GHz 处能够输出 42.32 W 的功率, 对应增益为 26.26 dB, 且均匀聚焦磁场只需 0.4 T.

关 键 词: 电子物理学; 卷绕微带线; 计算机仿真; 慢波结构; 行波管

中图分类号: O46 **文献标识码:** *A*

Received date: 2017-12-14, **revised date:** 2018-01-15 **收稿日期:** 2017-12-14, **修回日期:** 2018-01-15

Foundation items: Supported by the National Program on Key Basic Research Project of China (613233) and the National Natural Science Foundation of China (61771117, 61531010, 61271029)

Biography: DING Chong (1990-), male, Chengdu, doctoral candidate. Research area involves millimeter sources and vacuum electron devices. E-mail: morgoth@foxmail.com

* **Corresponding author:** E-mail: morgoth@foxmail.com, yywei@uestc.edu.cn

Introduction

Vacuum electron devices (VED) are employed for a number of specialized applications, such as satellite communications, radar, and medical apparatus [1-4]. New applications, such as high-data-rate communications and active imaging in the millimeter wave and submillimeter-wave bands, demand for reliable-performance high-power sources, and will be the driving force for vacuum electronics research in the near future. In particular, vacuum electronics could play a fundamental role in 5G mobile communications since the solid state devices cannot provide sufficient transmit power at millimeter-wave frequencies [5].

The traveling wave tube (TWT) can be a perfect solution to achieve long distance wireless connection with high data rate beyond 1 km in distance for point-to-multipoint communications [6]. The helix TWT [7, 8], as one of the most widely used VED, has the advantages of low operating voltage, wide operating bandwidth and high efficiency. Meanwhile, with the increase of the operating frequency, the size of the helix TWT reduces, which limits the use of the helix TWT up to a maximum operating frequency of 70 GHz. Also helix structures are very difficult to manufacture with high repeated precision, and the packing of the helix in to the waveguide and alignment with the electron beam are major challenges for helices with diameters below 1 mm [9].

2-dimensional (2D) slow wave structures (SWS), such as meander lines [10-13], have been proposed in order to simplify the realization of the helix TWT. The 2D SWS has the advantages of wide operating bandwidth and easy fabrication [14, 15], but still have issues to be solved before they can be fabricated as prototype devices. One of the main problems is that the sheet electron beam (SEB) operating at low voltage is used in most studied 2D SWS, which requires high magnetic focusing field that is very difficult to be realized with known magnetic materials compatible with vacuum tube fabrication [11, 16]. Thanks for the simple and mature technology, the cylindrical electron beam (CEB), which can be generated by a Pierce gun [17, 18] and focused by a periodic permanent (PPM) magnetic focusing system, can significantly simplify the fabrication of TWT devices.

This paper proposes a folded microstrip meander line (FMML) SWS that is suitable for cylindrical electron beam, which can effectively reduce the magnetic focusing system of the microstrip meander line SWS. A Ka band N-shaped FMML TWT with a magnetic focusing of only 0.4 T is set as an example, and the electromagnetic characteristics, transmission characteristics, and the beam-wave interaction of this modified MML SWS are investigated.

1 Description of the slow wave structure

The model of the FMML SWS is described in this section. As shown in Fig. 1(a), the traditional planar microstrip meander line (PMML) can be fabricated by printing a metal meander line on the flat surface of a rectangular substrate, and an SEB passes over the meander line in order to interact with the electromagnetic wave propagating along the meander line. This type of structure can achieve acceptable results only when the SEB is set to be closed to the metal meander line, which makes it difficult to focus the electron beam. Different from PMML SWS, a modified FMML SWS is proposed as shown in Fig. 1(b). The structure can be obtained by etching an arc shaped slot on the dielectric substrate [19-21] and printing the folded microstrip meander line in the slot. Because of the existence of the slot, the structure is very suitable for the CEB, which can efficiently reduce the focusing magnetic.

Figure 1 also shows the dimensional parameters of the two kind of MML SWS, where p is the length of a single pitch, w is the width of the metal meander line, t is the thickness of the metal meander line, a is the width of the dielectric substrate, r is the radius of the circle of the slot, h_d is the thickness of the dielectric substrate, θ is half of the arc angle.

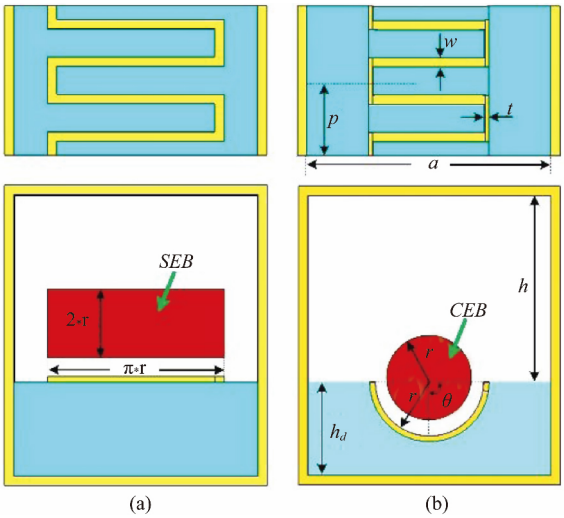

Fig. 1 Model and Dimensional parameters of (a) the PMML SWS and (b) the FMML SWS

图1 (a) 平面型微带慢波结构模型及参数. (b) 卷绕型微带慢波结构模型及参数

2 Analysis of the radio-frequency characteristics

In this section, the radio-frequency (RF) characteristics including dispersion characteristics and interaction impedances (Kc) are investigated, which are calculated by the Eigen-mode solver with master and slave boundaries in the 3-D electromagnetic simulation software Ansoft HFSS [22]. The interaction impedances can be calculated by

$$Kc = \frac{\left| \int_0^p E_z e^{-j\beta z} \mathrm{d}z / p \right|}{2\beta^2 p} \quad , \quad (1)$$

where E_z represents the longitudinal electric field, β is the longitudinal wave propagation constant, and p is the power flowing through the SWS cross-section.

The calculation models of the PMML SWS and

FMML SWS have been built, and all the parameters of the two structures are set the same as shown in Table 1. The frequency band focused on is Ka band, and the longitudinal bottom axial position of the sheet electron beam is 0.1 mm over the periodic metal meander line.

Table 1　The structural parameters of the FMML SWS and PMML SWS

表 1　卷绕型微带慢波结构和平面型慢波结构参数

Parameter	Value /mm
w	0.05
a	1.3
p	0.4
t	0.02
r	0.32
h	1
h_d	0.5
θ	180 (Deg)

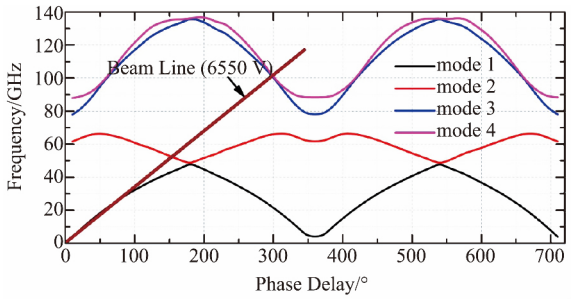

Fig. 2　The Brillouin curve (4 mode) of the FMML SWS

图 2　卷绕型微带慢波结构四个模式的布里渊曲线

Figure 2 shows the Brillouin curve (4 mode) of the FMML SWS. The 6 550 V beam line, which is the synchronizing voltage of the operating frequency of 35 GHz, intersects with the Brillouin curve of the high-order mode (mode 2, mode 3 and mode 4). This indicates that high-order mode oscillations may occur at this synchronous voltage. On the other hand, the interaction impedances of the operating frequency at 35 GHz is about 12 Ohms, while the interaction impedances of high-order mode corresponding to the frequency at the intersection point of the beam line is 1.8 Ohms, 0.2 Ohms and 0.18 Ohms, respectively. The coupling impedances of the high-order modes are much lower than that of the operating mode, so the probability of producing the high order mode oscillation is small. At the same time, an attenuator is further loaded in the process of the PIC simulation, which can further reduce the influence of high-order modes.

As shown in Fig. 3(a), the cold band-width of the FMML SWS ranges from 3.91 GHz to 46.19 GHz, while the cold band-width of the PMML SWS is in a range from 4.53 GHz to 47.64 GHz. Meanwhile, the FMML has lower normalized phase velocity and weaker dispersion, which means the FMML can have a wider operation band with a lower synchronous voltage. What's more, the interaction impedance of the FMML SWS ranges from 44.28 Ohms to 5.08 Ohms in the frequency range of

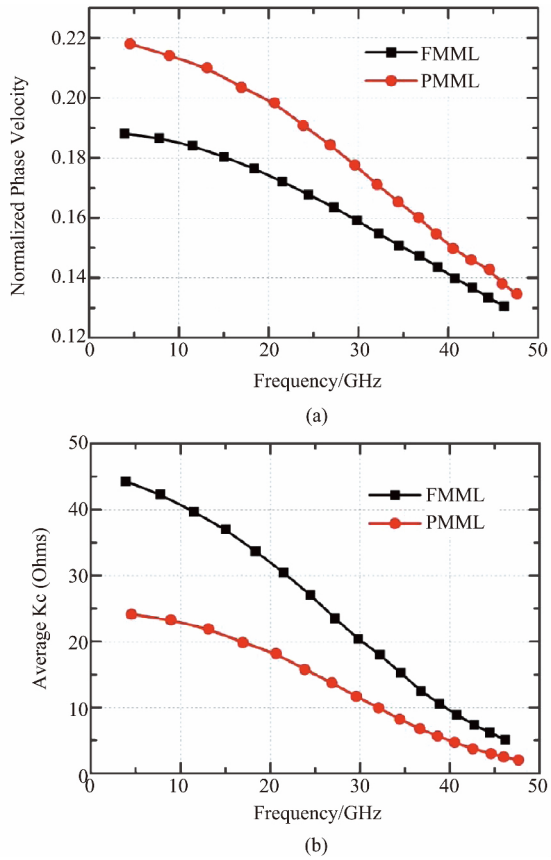

Fig. 3　(a) Dispersion properties and (b) average interaction impedances of the FMML SWS and the PMML SWS

图 3　(a) 卷绕型微带慢波结构和平面型微带慢波结构的色散特性对比. (b) 卷绕型微带慢波结构和平面型微带慢波结构的耦合阻抗对比

3.91 GHz to 46.19 GHz, and that of the PMML SWS ranges from 24.12 Ohms to 2.02 Ohms in the frequency range of 4.53 GHz to 47.64 GHz. It is obvious that the interaction impedance of the FMML SWS is much higher than that of the PMML SWS, which contributes an efficient energy exchange between the electron beam and the electromagnetic wave propagating in the FMML SWS.

Figure 4 shows the longitudinal electric field distribution of the PMML SWS and the novel FMML SWS. It is shown that the electric field is gathered to the central area of the FMML SWS, which contributes to higher interaction impedance of the FMML SWS.

3　Analysis of the transmission properties

The transmission properties of the proposed FMML SWS are calculated in this section. A circuit of 50 periods is built in CST Microwave Studio [23]. The material of the metal strip is set to be oxygen-free copper with conductivity of 2.25×10^7 S/m, and the material of the dielectric substrate is set as quartz glass with the relative permittivity of 3.78. As shown in Fig. 5, in the frequency range from 20 GHz to 40GHz, the transmission loss S21 is bigger than −5 dB and the reflection loss S11 is

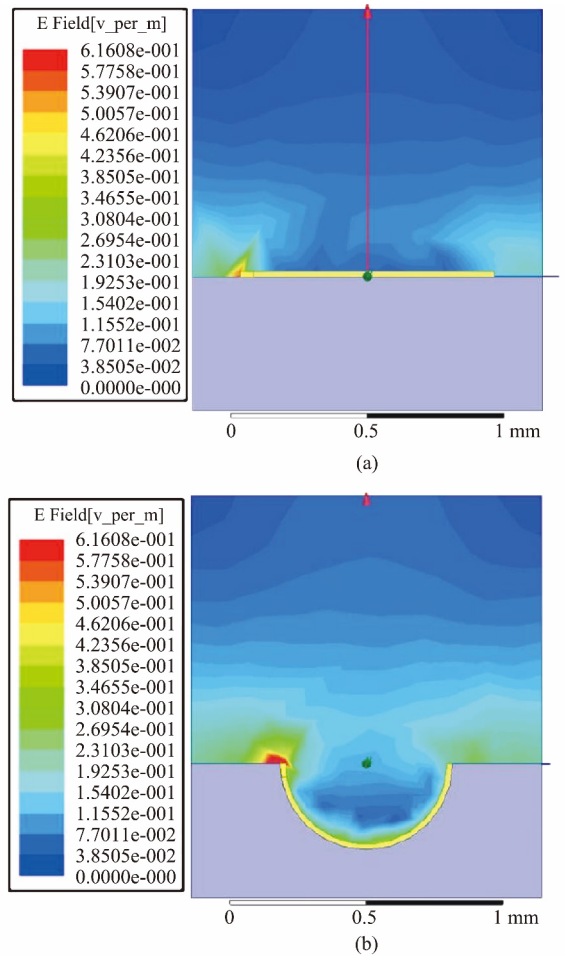

Fig. 4 (a) Longitudinal electric field distribution of the FMML. (b) Longitudinal electric field distribution of the PMML

图4 (a) 平面型微带慢波结构的纵向电场 E_z 分布. (b) 卷绕型微带慢波结构的纵向电场 E_z 分布

less than −17.4 dB.

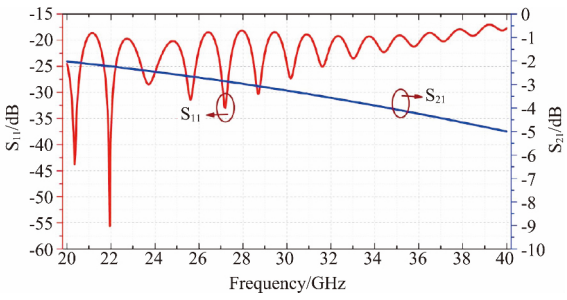

Fig. 5 Transmission characteristics of the FMML SWS

图5 卷绕型微带慢波结构的传输特性曲线

4 Analysis of the beam-wave interaction

Based on the simulated results including the radio-frequency characteristics and the transmission properties, a 3-D PIC model with the length of 120 pitches is built up as shown in Fig. 6. The intersection circuit is divided into two sections by an attenuator, and the length of each section is 40 and 66 pitches while the length of the attenuator is 14 pitches. Comprised by attenuation material, the attenuator can absorb the reflected wave and suppress the backward wave oscillation at a wide frequency range. On the other hand, a 3-D PIC model of the PMML TWT is also built. The optimized electrical parameters for both the Ka band TWTs are shown in Table 2. The focusing magnetic field of the PMML TWT is 0.6 T, while the focusing magnetic field of the FMML TWT is reduced to 0.4 T with a rate of 50%.

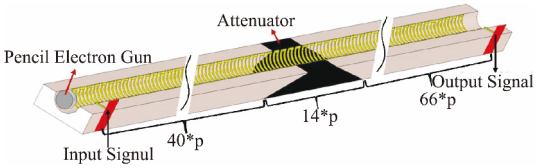

Fig. 6 3-D beam-wave interaction model of the FMML TWT

图6 卷绕型微带行波管的3维注波互作用模型

Table 2 Optimized electrical parameters of the FMML TWT and the PMML TWT

表2 优化后的卷绕型微带行波管和平面型微带行波管电参数

Parameter	Value of the FMML TWT	Value of the PMML TWT
Beam Voltage/V	6550	7700
Beam Current/A	0.1	0.1
Beam Cross Sectional Area/mm^2	π* 0.2^2	0.942* 0.4
Input Power/mW	100	100
Interaction Length /mm	48	67.2
Focusing Magnetic /T	0.4	0.6

Figure 7(a) shows the time-domain features of the input, output and reflected signal of the FMML TWT. As can be seen in Fig. 7(a), the output signal is steady after about 1.9 ns, and the reflected signal is small enough that can be ignored. That is to say, energy exchange between the electron beam and the drive signal is already stable. Figure 7(b) shows the frequency spectrum of the output signal obtained from the Fourier transformation. The results are normalized based on the maximum amplitude at 35 GHz. It is obvious that the normalized amplitude at 70 GHz (only 0.0054) is much lower than that at 35 GHz (set as 1). That means the modified FMML SWS is almost free from oscillation.

Figure 8 shows the output power along the axial direction of the FMML SWS. It can be seen that the signal is amplified gradually along the SWS and attenuated at 17.5 mm due to the function of the attenuator. Then, the signal is amplified again and outputs at the end of the SWS with a power of about 42 W.

Figure 9 shows the particle velocity modulation along the axial direction of the FMMLSWS. As shown in Fig. 9, most of the electrons are decelerated and a small number of electrons are accelerated, which means most

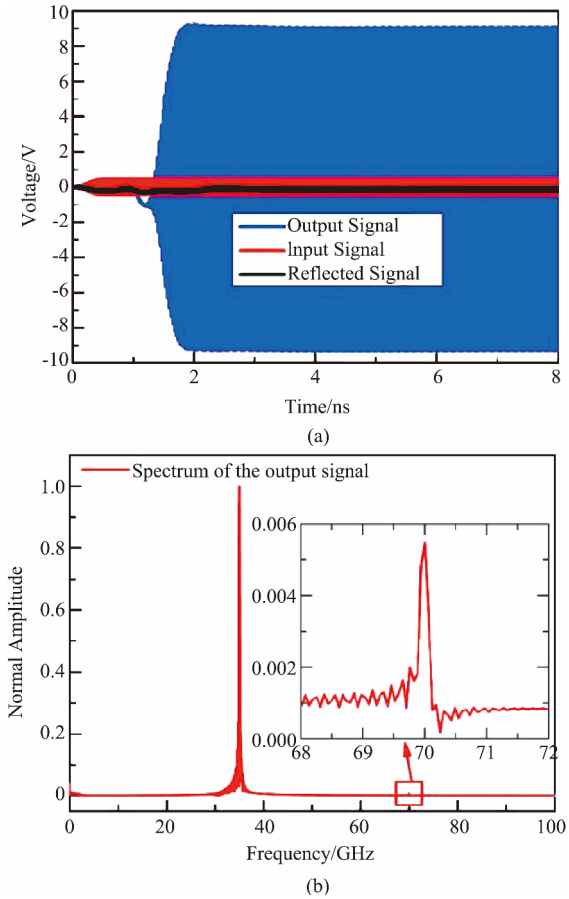

Fig. 7　(a) The input, reflected and output signal of the FMML TWT, (b) The frequency spectrum of the output signal at 35 GHz

图 7　(a) 卷绕型微带行波管的输入信号，反射信号及输出信号时域图，(b) 工作频点为 35 GHz 时的输出信号频谱图

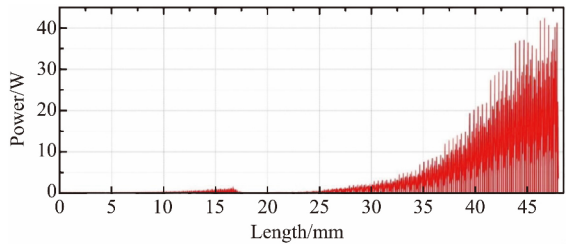

Fig. 8　Output Power versus longitudinal distance of the FMML TWT at 35 GHz

图 8　卷绕型微带行波管在 35 GHz 时输出功率沿着慢波结构纵向上的变化曲线

of the kinetic energy of the sheet electron beam is transferred to the high frequency electromagnetic field. Then the driving signal power will be amplified.

The frequency sweep is performed in order to examine the instantaneous bandwidth at a constant input power. Figure 10 gives the plots for output power and the corresponding gain versus drive frequency with the input power of 100 mW. As can be seen in Fig. 10(a), the

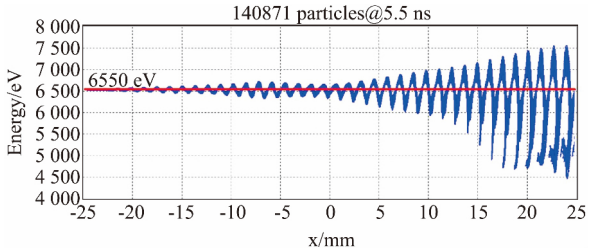

Fig. 9　Beam energy versus longitudinal distance of the FMML TWT at 35 GHz

图 9　卷绕型微带行波管在 35 GHz 时电子注能量在纵向的变化趋势

FMML TWT can deliver output power of more than 13.3 W at least covering the frequency range of 31 GHz to 37 GHz. The gain of the FMML TWT is higher than 21.24 dB at 31 ~ 37 GHz as shown in Fig. 10(b). Moreover, the peak output power is 42.32 W at 35 GHz, corresponding to the gain of 26.27 dB. Both the output power and gain of the FMML TWT are higher than those of the PMML TWT.

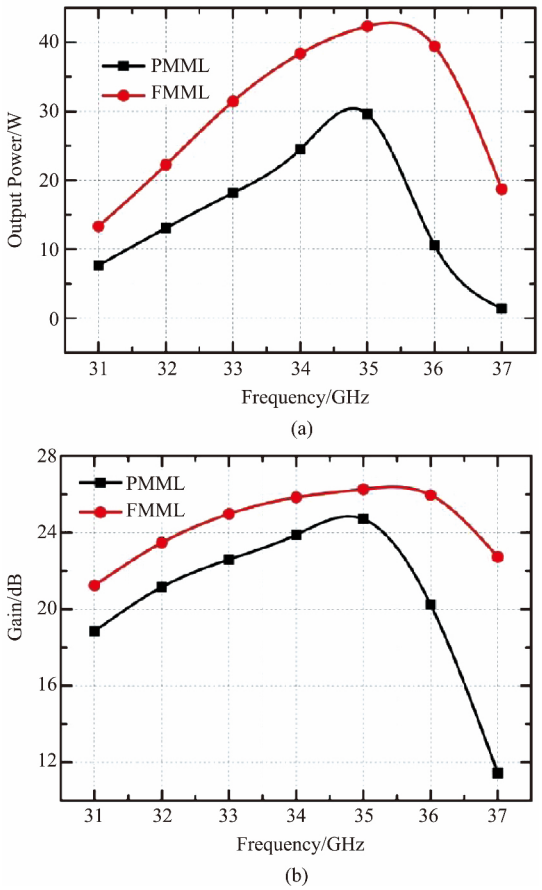

Fig. 10　(a) Output power and (b) gain versus frequency of the FMML TWT and PMML TWT

图 10　(a) 卷绕型微带行波管和平面型微带行波管的输出功率曲线对比，(b) 卷绕型微带行波管和平面型微带行波管的增益曲线对比

PIC simulations considering the actual circuit loss

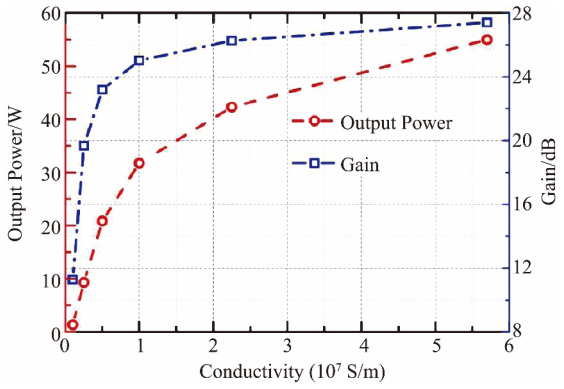

Fig. 11 Output power and gain dependence on conductivity of the metal meander line of the FMML TWT

图11 卷绕型微带行波管输出功率及增益随微带线电导率的变化趋势示意图

are performed. In general, the material with a conductivity of 2.25×10^7 S/m is used to estimate the circuit loss caused by the actual fabrication. Considering a probable larger surface roughness for the modified SWS and the actual assembly and fabrication situation, the material with lower conductivity is utilized for the interaction performance prediction. As shown in Fig. 11, when the conductivity lower than 1×10^7 S/m, the interaction performance of the FMML TWT becomes relatively poor. Therefore, in the process of practical processing, the conductivity of materials should be fully considered in order to obtain satisfactory results.

5 Conclusion

In this paper, a modified FMML SWS is proposed. The radio-frequency characteristics, transmission properties and the beam-wave interaction of the FMML SWS are analyzed. The proposed FMML SWS is suitable for cylindrical electron beam TWTs, which can efficiently reduce the focusing magnetic. Furthermore, this novel slow-wave circuit can be well integrated with the solid-state circuit, which could be an attractive candidate for the millimeter wave power module (MMPM).

References

[1] Qiu J X, Levush B, Pasour J, *et al*. Vacuum Tube Amplifiers [J]. *IEEE Microwave Magazine*, 2009, **10**(7): 38-51.

[2] Chong C K, Cordrey D A, Dawson R C, *et al*. High Power Millimeter Wave Helix TWT Programs at L-3 ETI [C]. *IEEE 14th International Vacuum Electronics Conference*, 2013: 1-2.

[3] Ehret P, Laurent A, Bosch E. Broadband Traveling Wave Tubes in Ka and Ku Band [C]. *IEEE 15th International Vacuum Electronics Conference*, 2014: 47-48.

[4] Gong H, Xu J, Tang T, *et al*. A 1 kW 32 ~ 34 GHz Folded Waveguide Traveling Wave Tube [J]. *IEEE Transactions on Plasma Science* 2014, **42**(1): 8-12.

[5] Alavi S E, Soltanian M R K, Amiri I S, *et al*. Towards 5G: A Photonic Based Millimeter Wave Signal Generation for Applying in 5G Access Front haul [J]. *Scientific Reports*, 2016, **6**: 1-11.

[6] Paoloni C, Magne F, André F, *et al*. Millimeter wave wireless system based on point to multipoint transmissions [C]. *The European Conference on Networks and Communications*, 2016: 106-110.

[7] Ghosh S, Sinha A K, Gupta R K, *et al*. Space-harmonic effects in helical slow-wave structure-An equivalent circuit analysis – Abstract [J]. *Journal of Electromagnetic Waves and Applications*, 2000, **14**(8): 1083-1085.

[8] Liu L, Wei Y, Xu J, *et al*. A Novel Slotted Helix Slow-wave Structure for Millimeter-wave Traveling-wave Tube [J]. *Progress in Electromagnetics Research-Pier*, 2013, **135**(10): 347-362.

[9] Ulisse G, Krozer V. W-Band Traveling Wave Tube Amplifier Based on Planar Slow Wave Structure [J]. *IEEE Electron Device Letter*, 2017, **38**(1): 126-129.

[10] Shen F, Wei Y, Xu X, *et al*. Symmetric Double V-Shaped Microstrip Meander-Line Slow-Wave Structure for W-Band Traveling-Wave Tube [J]. *IEEE Transections on Electron Devices*, 2012, **59**(5): 1551-1557.

[11] Shen F, Wei Y, Yin H, *et al*. A Novel V-Shaped Microstrip Meander-Line Slow-Wave Structure for W-band MMPM [J]. *IEEE Transactions on Plasma Science*, 2012, **40**(2): 463-469.

[12] Wang S, Gong Y, Hou Y, *et al*. Study of a Log-Periodic Slow Wave Structure for Ka-band Radial Sheet Beam Traveling Wave Tube [J]. *IEEE Transactions on Plasma Science*, 2013, **41**(8): 2277-2282.

[13] Ding C, Wei Y., Li Q, *et al*. A dielectric-embedded microstrip meander line slow-wave structure for miniaturized traveling wave tube [J]. *Journal of Electromagnetic Waves and Applications*, 2017, **31**(17): 1938-1946.

[14] Sengele S, Jiang H, Booske J H, *et al*. A Selectively metallized, microfabricated W-band meander line TWT circuit [C]. *IEEE International Vacuum Electronics Conference*, 2008: 18-19.

[15] Sengele S, Jiang H, Booske J H, *et al*. Microfabrication and Characterization of a Selectively Metallized W-Band Meander-Line TWT Circuit [J]. *IEEE Transections on Electron Devices*, 2009, **56**(5): 730-737.

[16] Guo G, Wei Y, Zhang M, *et al*. Novel Folded Frame Slow-Wave Structure for Millimeter-Wave Traveling-Wave Tube [J]. *IEEE Transections on Electron Devices*, 2013, **60**(11): 3895-3900.

[17] Sharma R K, Sinha A K, Joshi S N. An improved method for the synthesis of anode aperture for Pierce guns [J]. *IEEE Transections on Electron Devices*, 2001, **48**(2): 395-397.

[18] Sharma R K, Srivastava V. Low convergent confined-flow Pierce gun for a space TWT [J]. *International Journal of Electronics*, 2004, **91**(2): 97-105.

[19] Zhang X Y, Yi X J, He M, *et al*. Large-area quartz glass microlens array fabricated by ion beam etching for focal plane detectors [J]. *Journal of Infrared and Millimeter Waves*, 1999, **18**(2): 97-102.

[20] Tang Y H, Lin Y H, Shiao M H, *et al*. Development of thin quartz glass utilising through-glass-via (TGV) formation by dry etching technology [J]. *Micro & Nano Letters*, 2016, **11**(10): 568-571.

[21] Gottmann J, Hermans M, Repiev N, *et al*. Selective Laser-Induced Etching of 3D Precision Quartz Glass Components for Microfluidic Applications-Up-Scaling of Complexity and Speed [J]. *Micromachines*, 2017, **8**(4): 1-10.

[22] Ansoft Corp. Ansoft HFSS User's Reference [OL]. Available: *http://www.ansoft.com.cn/*.

[23] CST Corp. CST MWS Tutorials [OL]. Available: *http://www.cst-china.cn/*.